

Lithostratigraphy and petrology of Lachman Crags and Cape Lachman lava-fed deltas, Ulu Peninsula, James Ross Island, north-eastern Antarctic Peninsula: Preliminary results

Şafak Altunkaynak^{1*}, Ercan Aldanmaz², Işıl Nur Güraslan¹, Ayşe Zeynep Çalışkanoğlu¹, Alp Ünal¹, Daniel Nývlt^{3,4}

¹*Department of Geological Engineering, Istanbul Technical University, Maslak 34469, Istanbul, Turkey*

²*Department of Geology, University of Kocaeli, 41380 Izmit, Turkey*

³*Department of Geography, Faculty of Science, Masaryk University, Kotlářská 2, 611 37 Brno, Czech Republic*

⁴*Czech Geological Survey, Brno branch, Leitnerova 22, 658 69 Brno, Czech Republic*

Abstract

This paper presents the preliminary results regarding the lithostratigraphy, petrography and petrology of James Ross Island Volcanic Group dominating the Lachman Crags and Cape Lachman lava-fed deltas in the Ulu Peninsula, James Ross Island north-eastern Antarctic Peninsula. Studied lava-fed deltas were produced via Late Miocene to Pleistocene sub-marine and sub-glacial volcanism and made up four main lithofacies: a-bottomset pillow lavas, peperites and associated volcanoclastic/siliciclastic deposits; b-foreset-bedded hyaloclastite breccias; c- intrusions (feeder dykes, sills, and plugs) and d-topset subaerial lavas. Collectively these lithofacies record the transition from an effusive subaqueous to an effusive subaerial eruption environment. All lava samples and dykes from bottomset, foreset and topset lava-fed delta associations are olivine-phyric alkali basalts and are mineralogically and geochemically homogeneous. These eruptive products display significant enrichments in alkali contents and have ocean island basalt (OIB)-type, intra-plate geochemical signatures characterized by enrichments in all highly to moderately incompatible trace elements relative to basaltic rocks from ocean ridge settings. Volcanic products from a number of different eruptive periods display limited variations in major and trace element relative abundances, indicating derivation from a relatively homogeneous mantle source. The results of quantitative modelling of geochemical data is consistent with the view that the primary melts from which these mafic alkaline rocks were originated are the products of relatively small degrees (~3-7%) of partial melting of a volatile-bearing, metasomatized mantle source. The magmatism is likely the result of extension-driven mantle upwelling.

Received July 19, 2018, accepted September 7, 2018.

*Corresponding author: S. Altunkaynak <safak@itu.edu.tr>

Acknowledgements: This study was carried under the auspices of Turkish Republic Presidency, supported by the Ministry of Science, Industry and Technology, and coordinated by Istanbul Technical University (ITU) Polar Research Center (PolReC). Field study on James Ross Island was undertaken within the scope of TAEII, Turkey-Czech Republic Bilateral Cooperation, and a collaborative research between Istanbul Technical University and Masaryk University in Brno. We would like to express our special thanks to the expedition members and crew of the J.G. Mendel Station for their friendship and logistic support during the field campaign (January-March 2018). The facility of the J.G. Mendel Station is supported by the Ministry of Education, Youth and Sports of the Czech Republic projects no. LM2015078 and CZ.02.1.01/0.0/0.0/16_013/0001708. We also thank the anonymous reviewers for their careful reading of our manuscript and their insightful comments and suggestions.

Key words: Antarctica, James Ross Island, Lava-fed delta, lithostratigraphy, petrology

DOI: 10.5817/CPR2018-1-5

1. Introduction

Lava-fed deltas (LFDs) formed by lava intrusion beneath ice or water represent one of the distinctive sub-glacial/sub-marine volcanic landforms with characteristic morphology and internal stratigraphy (Jones et al. 1970, LeMasurier 2002, Skilling 2002, 2009; Umino et al. 2006, Mitchell et al. 2008, Smellie et al. 2008, 2013; Smellie et al. 2016). Morphologically, LFDs differ from the other volcanic landforms with their steep slopes and a flat top. In most places, LFDs display bipartite or tripartite internal stratigraphy that consists of sub-aqueous/sub-glacial lithofacies (subhorizontal bottomsets, steep foreset-bedded hyaloclastite breccias, and pillow lavas) overlain by subaerial horizontally-bedded topset lavas with a passage zone between them (Jones et al. 1970, Skilling 2002, Smellie et al. 2006, 2008). Passage zone between subaerial and subaqueous/sub-glacial lithofacies indicates the ice/water paleo-level, which provides important information about palaeoenvironmental and palaeoclimatic conditions (Edwards et al. 2002, Smellie et al. 2008, 2013). Although their occurrence is rare compared to the other volcanic edifices worldwide, many characteristics of lava-fed deltas are well documented especially in Iceland (*e.g.* Sigvaldason 1968, Tuffen et al. 2002, Skilling 2009) and Antarctica (*e.g.* Nelson 1975, Smellie 1987, 2006; Skilling 1994, 2002; Wilch et al. 2007, Smellie et al. 2006, 2008, 2013; Nehyba et al. 2015).

Excellent exposures of lava-fed deltas crop out along several parts of the James Ross Island, north-eastern Antarctic Peninsula (*see* Figs 1, 2). They represent the initial stages of sub-glacial/sub-marine eruptions of the Mount Haddington stratovol-

cano (1630 m high and 60 km wide), which has built the island throughout the Miocene-Holocene (Nelson 1975, Pirrie et al. 1987, Sykes 1988, Skilling 1994, Smellie et al. 1994, Smellie et al. 2006, 2008; Hambrey et al. 2008, Nelson et al. 2009). The whole volcanic suite of this area is known as the James Ross Island Volcanic Group (JRIVG) and consists of various types of volcanic rocks: hyaloclastites, basaltic lavas, dykes and subordinate pyroclastic rocks. The James Ross Archipelago is one of the best-studied areas in terms of physical volcanology and geochronology of lava-fed deltas in Antarctica (*e.g.* Nelson 1975, Pirrie et al. 1987, Smellie, 1987, 2006; Sykes 1988, Porębski et al. 1990, Skilling 1994, Smellie et al. 1994, Kristjánsson et al. 2005, Smellie et al. 2006, 2008, 2013; Hambrey et al. 2008, Nelson et al. 2009).

In recent years, a large number of studies have been undertaken to contribute to the existing knowledge, regarding especially the sedimentological features of clastic and volcano-clastic deposits associated with subglacial volcanism, lava-fed delta evolution and the phases of volcanic inactivity (Nývlt et al. 2011, Nehyba et al. 2014, 2015; Mlčoch et al. 2018). Petrological characteristics of the JRIVG rocks have also been investigated in some detail (Smellie 1987, Košler et al. 2009, Bastias et al. 2012, Calabozo et al. 2015), although relevant data for a detailed geochemical interpretation of the volcanic exposures is limited. Based on the available data, previous studies have described the JRIVG as the products of a back-arc basin magmatic activity developed in response to slab rollback induced lithospheric extension (Košler et al. 2009, Calabozo et al. 2015).

2. Geological overview

The James Ross Island volcanic field is located in the north-eastern part of the Antarctic Peninsula between 63°45'–64°30' S and 58°30'–57°00' W (Fig. 1). A large area in the field is covered by the Late Miocene to Late Pleistocene alkaline volcanic rocks (Barker 1982, Smellie 1987, Larter et Barker 1999, Barker et al. 2003, Smellie et al. 2006, 2008). The lavas on James Ross Island and other small islands in the Prince Gustav Channel, separating James Ross Island from Antarctic Peninsula, mainly emplaced on the Jurassic to Paleogene sedimentary rocks of the James Ross Basin. This basin is considered to be a back-arc rift basin developed in association with the formation of Mesozoic magmatic arc of the Antarctic Peninsula (Barker et al. 2003, del Valle et Scasso 2004).

Numerous volcanic rocks of sub-glacial and sub-aerial origin (JRIVG) exist in the north-eastern part of the Antarctic Peninsula (James Ross, Vega, Corry, Eagle and Tail islands - Fig. 1). The magmatic products of the JRIVG unconformably overlie the Cretaceous marine sediments (*e.g.* Bibby 1966, Crame et al. 1991) and spread over a large area of ~6000 km² in James Ross Archipelago, but the most extensive outcrops are seen on James Ross Island and Vega Island (Nelson 1975, Kristjánsson et al. 2005, Smellie et al. 2006, 2008; Košler et al. 2009, Calabozo et al. 2015).

With an areal extent of 2500 km², James Ross Island is the largest island of the eastern coast of Antarctic Peninsula, and at least 50 effusive eruptions described from here preserved mainly as LFD (Smellie et al. 2006, 2008). The eruptive products are suggested to have been sourced and travelled from the Mount Haddington strato-volcano during the Late Miocene till Late Pleistocene (Smellie et al. 2006). The published K/Ar and Ar/Ar ages yielded an age range of 6.7–0.13 Ma for the JRIVG (Rex 1976, Massabie et Morelli 1977, Sykes 1988, Lawver et al. 1995, Jonkers et al.

2002, Kristjánsson et al. 2005, Smellie et al. 2006, 2008; Nývlt et al. 2011, Nehyba et Nývlt 2014), although Marensi et al. (2010) reported that the volcanic activity on the island might have initiated ~12 m.y. ago.

Several individual LFDs produced bottomsets made of reworked glaciogenic, glaciomarine and marine deposits on James Ross Island in the Late Miocene and Pliocene (Smellie et al. 2013, Nehyba and Nývlt, 2015). The thicknesses of LFDs vary between 100 and 600 m (generally 100–250 m; Smellie et al. 2008). Hyaloclastite breccias (foreset) comprise more than 60% of the total thickness, while horizontal subaerial lavas (topset) are generally 25–50 m thick (max. 150–185 m; Smellie et al. 2006, 2008). One of the oldest deltas with ages between 5.32 and 3.95 Ma (basal delta and upper delta of Lachman Crag, respectively) is preserved in the Ulu Peninsula and is known as Lachman Crag superimposed delta (Nelson 1975, Sykes 1988, Smellie 1999, 2006; Smellie et al. 2006, 2008; Nehyba et Nývlt, 2015). It contains the thickest topset subaerial lava (185 m) that includes also relatively thick, coarse-grained horizontal lava flows above a nearly horizontal passage zone (Smellie et al. 2008). In our study area, the northern part of the Ulu Peninsula (Fig. 1), the best sectors showing the lithostratigraphic sequence of LFD are Cape Lachman, Johnson Mesa, Berry Hill and Lachman Crag. According to Smellie et al. (2008), these sectors represent basal, main and upper deltas of “Lachman Crag superimposed lava-fed delta” (LCLFD), respectively. However, it should be noted that a more recent study of Nývlt et al. (2011) showed that the Cape Lachman and Lachman Crag volcanic edifices are separated by >80 m thick glaciogenic to marine Mendel Formation. Therefore, the Cape Lachman lava-fed delta is described separately. LCLFD, which exhibits an almost north-south longitudinal orientation and the

length of ~12 km (Figs 1, 2), represents an unique example of marine/glaciomarine setting LFD on the island (Nelson 1975, Smellie et al. 2006, 2008; Nehyba et Nývlt

2014, 2015) and probably one of the longest lava-fed deltas in the world (Mlčoch et Nývlt 2013).



Fig. 2. Lachman Crags delta from East to West. *Symbols:* C: Cape Lachman, B: Berry Hill, S: Smellie Peak.

3. Materials and Methods

Fieldwork focused on lithofacies and geometric description of individual rock types and their relationships on natural outcrops on James Ross Island. Thin sections of representative rock samples were studied under the polarising microscope to describe the nature of groundmass, phenocrysts and xenoliths from the petrographical point of view. Subsequently, we selected the best-preserved volcanic rock samples with no signs of alteration for geochemical analyses. External surfaces of the samples were removed by splitting the samples into chips, which were then ground to a powder in an agate ball mill. Rock samples were analysed for their whole-rock major oxides using X-ray fluorescence (XRF) at the ACME Analytical Laboratories in Vancouver, Canada (package code: XF700). Major oxide

abundances were measured on fused discs. Loss on ignition was determined by heating a separate aliquot of rock powder at 900°C for > 2 h. The same samples were also analysed for trace element concentrations at the Department of Geology, University of Kocaeli. Rock powders were first fused to ensure dissolution of all phases and then dissolved in hot HF and HNO₃ to prepare the solution, from which trace element abundances were determined using inductively coupled plasma mass spectrometry (ICP-MS; Perkin Elmer Elan DRC-e). Whole-rock major and trace element data for the samples are presented in Table 1. We used the GCDkit of Janoušek et al. (2006) to generate the diagrams for geochemical interpretations.

4. Lithostratigraphy and description of volcanic lithofacies

Lachman Crags superimposed lava-fed delta and Cape Lachman lava-fed delta are made up of four main lithofacies: a- bottom-set pillow lavas, peperites and associated

volcaniclastic/siliciclastic deposits; b- fore-set-bedded hyaloclastite breccias; c- intrusions (feeder dykes, sills, and plugs); d- top-set subaerial lava flows.

Sample	JR-12	JR-31	JR-32	JR-51	JR-54	JR-64	JR-98	JR-102	JR-104	JR-109	JR-111	JR-113	C-4
Locality													
SiO₂	48.20	47.00	48.10	48.15	48.90	49.00	49.50	48.30	47.50	47.40	45.58	48.80	48.70
TiO₂	1.80	2.00	1.75	1.70	2.15	1.84	1.75	1.77	1.75	1.73	1.90	1.85	1.70
Al₂O₃	16.30	14.80	15.40	15.19	16.60	16.60	15.40	15.50	15.40	15.40	14.95	16.20	15.60
Fe₂O₃	11.00	11.60	11.90	11.23	10.90	9.80	11.80	12.10	12.00	11.80	12.29	10.80	11.70
MnO	0.16	0.16	0.17	0.15	0.15	0.14	0.16	0.17	0.16	0.16	0.15	0.15	0.16
MgO	7.37	10.60	8.58	11.34	5.64	5.02	8.38	8.88	9.64	9.41	7.05	6.86	8.46
CaO	9.27	8.27	8.59	4.06	8.97	8.35	7.95	8.71	7.81	7.46	11.87	8.85	8.25
Na₂O	3.80	3.35	3.40	4.62	4.20	4.02	3.78	3.19	3.54	3.92	3.26	3.88	3.84
K₂O	0.91	0.97	1.01	1.97	1.23	1.76	1.37	1.10	1.38	1.51	1.08	1.04	1.02
P₂O₅	0.36	0.55	0.31	0.48	0.40	0.52	0.42	0.32	0.55	0.62	0.47	0.34	0.35
L.O.I	0.10	0.30	0.10	1.07	0.70	2.60	0.50	0.20	0.10	0.20	1.35	0.60	0.10
Total	99.31	99.66	99.15	98.89	99.86	99.67	100.05	100.29	99.89	99.66	98.65	99.42	99.93
Cr	261.08	379.49	299.94	272.46	146.45	113.31	256.74	285.06	350.49	286.07	286.43	268.66	373.14
V	229.19	183.27	194.72	147.36	212.45	185.54	154.69	180.39	132.49	122.28	137.85	180.82	204.27
Ni	107.62	223.28	156.05	150.58	50.06	32.91	137.19	160.97	244.58	236.88	196.25	111.70	180.91
Co	49.71	59.05	51.18	44.41	36.91	34.84	54.93	51.15	56.70	50.67	49.12	42.95	53.78
Cu	45.36	40.82	42.57	34.62	33.28	27.14	31.45	40.22	41.76	42.25	34.35	37.03	43.45
Rb	15.14	7.76	14.64	15.28	19.53	20.55	17.61	12.23	8.83	11.12	6.49	14.09	15.13
Sr	540.68	656.50	444.65	427.65	488.16	987.90	537.67	469.98	682.39	651.13	890.64	415.77	477.71
Y	26.06	23.69	23.40	17.62	25.18	23.53	23.08	22.58	21.27	20.39	16.90	22.49	24.63
Zr	187.08	191.78	149.41	151.32	173.88	198.03	180.76	146.23	169.55	218.42	176.19	159.12	172.41
Nb	25.09	33.41	24.42	25.34	26.13	38.94	31.54	23.59	35.66	35.76	26.22	23.97	27.18
Ba	132.26	141.73	140.74	142.08	152.22	211.62	158.72	140.29	143.07	141.17	124.25	161.64	143.40
La	17.65	23.32	14.13	18.79	18.03	24.95	19.63	13.62	23.73	25.28	17.77	14.66	16.74
Ce	37.42	49.44	30.83	38.46	38.81	50.66	39.64	29.65	48.37	50.95	37.57	31.38	35.27
Pr	4.59	5.93	3.90	4.55	4.75	5.89	4.66	3.73	5.60	5.85	4.54	3.96	4.37
Nd	19.81	23.98	17.44	18.54	20.48	24.21	19.57	16.55	23.37	24.09	19.00	17.66	18.71
Sm	4.89	5.64	4.30	4.02	5.11	5.72	4.91	4.10	5.39	5.36	4.68	4.60	4.54
Eu	1.69	1.87	1.52	1.39	1.75	1.86	1.65	1.45	1.73	1.76	1.51	1.54	1.57
Gd	5.28	5.75	5.06	4.18	5.40	5.57	5.05	4.62	5.26	5.23	4.41	4.95	5.01
Tb	0.88	0.88	0.85	0.66	0.85	0.85	0.83	0.78	0.81	0.82	0.66	0.81	0.83
Dy	5.07	4.68	4.74	3.59	5.12	4.63	4.65	4.49	4.39	4.38	3.65	4.59	4.69
Ho	1.02	0.92	0.93	0.70	1.06	0.93	0.93	0.92	0.87	0.85	0.68	0.93	0.95
Er	2.81	2.41	2.64	1.88	2.70	2.51	2.40	2.48	2.36	2.25	1.72	2.43	2.51
Tm	0.39	0.34	0.37	0.26	0.38	0.36	0.34	0.34	0.31	0.31	0.24	0.34	0.36
Yb	2.46	2.16	2.29	1.65	2.31	2.21	2.10	2.13	1.93	1.90	1.44	2.17	2.25
Lu	0.37	0.30	0.33	0.24	0.34	0.33	0.32	0.32	0.28	0.28	0.19	0.31	0.33
Hf	5.48	5.61	4.88	4.42	5.35	5.82	5.65	4.82	5.56	6.66	5.20	5.08	5.22
Ta	1.80	2.47	1.81	1.85	1.91	2.65	2.32	1.81	2.72	2.73	2.03	1.80	1.93
Pb	2.42	2.65	3.40	3.00	2.79	3.72	2.86	3.52	2.38	2.83	1.87	2.74	4.46
Th	2.87	3.11	2.62	3.23	3.04	4.16	3.91	2.59	3.16	3.81	2.37	2.74	2.96
U	0.74	0.91	0.72	0.86	0.81	1.11	1.06	0.69	0.60	0.97	0.69	0.69	0.82

Table 1. Whole-rock major oxide and trace element compositions for the alkaline volcanics of JRIVG.

a- Bottomset pillow lavas and associated deposits

Closely packed pillow lavas form the basal section of the Cape Lachman lava-fed delta and are best observed along the eastern slopes of Cape Lachman from the Herbert Sound coast (Fig. 3a). In this area, they are mostly interfingered with auto-breccias, peperites, and hyaloclastite/volcanosedimentary deposits and cut by feeder dykes with the same composition. The thickness of this basal lithofacies (pillow lava-breccia, peperite and volcanoclastic sediments) of LFD is variable. The lavas are overlain by hyaloclastite breccias.

The peperites are seen in Cape Lachman and eastern/southeastern flanks of Bery hill. They are represented by blocky peperites occurring along the contacts between the host volcanosedimentary deposits and basaltic feeder dykes/intrusions (Fig. 3b) and pillow lavas as a result of interaction of hot magma with host sediment during the subaqueous magmatic activity. Blocky peperites include isolated dolerite/pillow basalt fragments of variable sizes ranging from mm to meters set in the fine- to medium-grained, pinkish/light brown to yellow sandy matrix. The volcanosedimentary host comprises reworked tuff (tuffaceous sediment) and volcanogenic sandstone/mudstone. The aphanitic pillow basalts and doleritic feeder dykes display thin chilled margin in contact with sediments. Some feeder dykes were brecciated by in situ quench fragmentation (Fig. 3b), and they also deform host sedimentary structures, locally. Angular-subangular pillow basalt-dolerite fragments, in some places, form a jigsaw-fit structure within the fine-grained matrix supporting in situ fragmentation. The basalt-dolerite fragment/fine-grained sedimentary matrix ratio and intensity of deformation in host sediment decrease sharply away from the contact with the pillow lava/feeder dyke intrusion.

Pillow lavas and their isolated lobes

within the peperites and hyaloclastites are usually aphanitic in texture. They display well-developed radial joints, multiple concentric rusty rind structures, highly vesiculated cores with poorly or none vesiculated glassy rims, and hollows in their cores. The vesicles are usually filled by zeolite minerals. Based on their morphology, two types of pillow lavas are identified in the pillow lava succession: a. Corrugated closely packed pillow lavas devoid of any inter-pillow hyaloclastite/sediments representing the proximal lowermost part of the pillow succession (Fig. 3c). b. Non- (or not strongly) corrugated dispersed pillow lobes with inter-pillow sediment/hyaloclastite representing relatively upper parts and/or distal domain of the succession (Fig. 3d). The plunge of central and proximal pillow lava piles is low ($<15^\circ$; Fig. 3c), while that of distal pillows are relatively steeper ($>15^\circ$).

Pinkish- to yellow-pale brown coloured, fine to medium grained tuffaceous sediments, tephra and hyaloclastites showing crudely- to well-developed, nearly horizontal bedding gradually accumulate on top of the pillow lava-breccia-peperite succession and are cut by intrusions (feeder dykes and apophyses) associated with the pillow lavas (Fig. 3a, b, c and e). They also include pillow fragments of variable size. Closely-packed pillow lavas and peperites, those are common in Cape Lachman, gradually disappear towards the south and are replaced by matrix-supported fine- to medium-grained hyaloclastites (reworked hyaloclastites, volcanosedimentary rocks, Fig. 4a). Bottomsets of LCLFD in Berry Hill (Fig. 4a) and Lachman Crags areas are represented by relics of basalt flows/sills, volcanic debris flows, traction current sediments and glaciogenic deposits, which are described in detail by Nehyba and Nývlt (2015). Therefore, sedimentary bottomsets are not discussed here in detail.

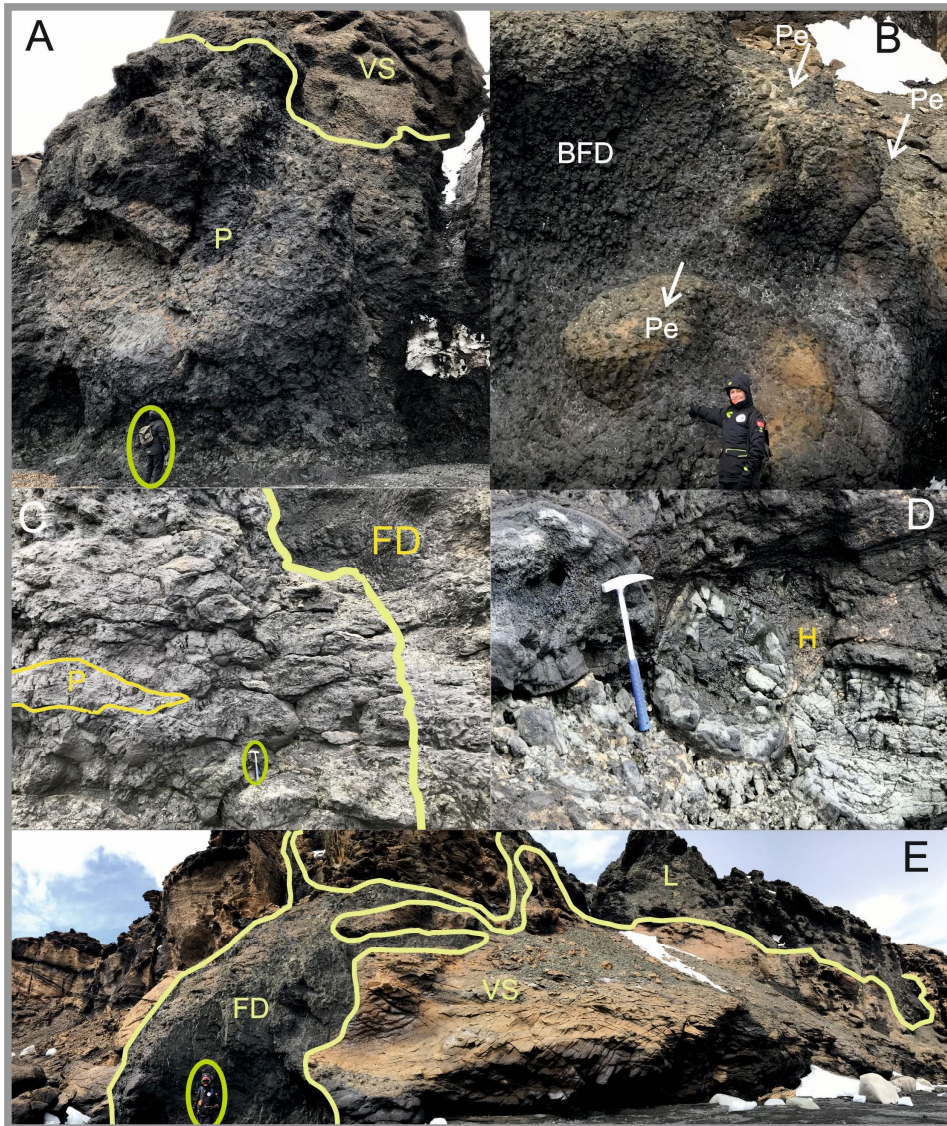


Fig. 3. A- Closely packed pillow lavas observed in the eastern slopes of Cape Lachman. Please note that pinkish-pale brown tuffaceous sediment (VS) on top of the pillow (P) succession; B- Blocky peperite (Pe) occurred along the contact between host sediment and brecciated feeder dyke (BFD); C- Corrugated closely packed pillow lavas (P) devoid of any inter-pillow hyaloclastite/sediments cutting by feeder dyke (FD); D- Non(slightly)-corrugated pillow lobes with inter-pillow hyaloclastite (H). Please note that highly vesiculated core and hollow development within pillow lobe on the left side; E- Dyke (FD) feeding a pillow lava flow (L) at the Cape Lachman coast (VS: volcanosedimentary rocks).

b- Lava-fed foreset-bedded hyaloclastite breccias

Quench fragmented lava-fed hyaloclastite breccias with steeply dipping foreset-bedding is the most typical and remarkable lithofacies of LCLFD in James Ross Island. Their dip direction is usually N-NE with an dipping angle of up to 40° (Fig. 4a, c). The hyaloclastite breccias are medium to coarse-grained and poorly sorted. They consist almost entirely of angular, dark pillow lava fragments (Fig. 4b) and lobes set in an orange/brown matrix. The size of the pillow fragments and the lobes within the matrix ranges from pebble to block. At some places (*e.g.* northern and eastern slopes of Berry Hill), hyaloclastite breccias contain isolated megapillows (up to 15 m in size) with well-developed radial joints

and glassy margins. Beneath the topset, a horizontal hyaloclastite-lava complex was identified as multiple and long lava lobes/tongues, which are sandwiched between hyaloclastite breccia layers (*e.g.* at southern Lachman Crags). These lava lobes are generally aphanitic in texture when compared to the overlying coarser-grained subaerial lavas. The length and thickness of black-to grey-coloured elongated lava layers are rather changeable even in the same outcrop. Lava layers and crudely-bedded hyaloclastite breccia association close to the contact between foreset and topset lithofacies represent the passage zone between subaqueous and subaerial conditions.

c- Intrusions (feeder dykes, sills and plugs)

This lithofacies consists mainly of linear dykes, sills, irregular shaped intrusions and chimneys/plugs. They are all basaltic in composition and display doleritic texture. They cut the entire volcanic/volcanoclastic succession (except for the subaerial lava caps) and the Cretaceous sediments of James Ross Basin. Although cross-cutting contact relationships indicate that the dykes are younger than the pillow lavas and foreset-bedded hyaloclastite breccias, most of these intrusions are considered as feeder dykes of bottomset pillow lavas (Fig. 3e) and lava lobes/tongues within the foreset-bedded hyaloclastite breccias, because they not only cut across the pillow lavas and lava lobes/tongues within the foreset bedded

hyaloclastite breccias, but also interfinger with them (*e.g.* at Cape Lachman and Berry Hill, Fig. 3e). Most of the intrusions exhibit radial and strike parallel joints, the feeder dykes at some places are pillowed and display ball-chain structures.

Volcanic plugs and chimneys are also abundant features in other parts of Ulu Peninsula (*e.g.* between J. G. Mendel Station and Bibby Hill, north-east of Stoneley Point and on Santa Marta Slopes). Usually, the plugs/chimneys and the major dykes are aligned primarily along a WNW-ESE direction perpendicular to the orientation of LCLFD and are considered as local/secondary eruption centres around the Mount Haddington stratovolcano.

d- Topset subaerial lava flows

The subaerial lava flows represent the topsets of lava-fed deltas, which are often fragmented (*e.g.* at Johnson Mesa) and/or eroded (*e.g.* at Cape Lachman). They are represented by nearly horizontal lava sheets overlying the foreset bedded hyaloclastite

breccia (Fig. 4c). They consist of thin pahoehoe lava flows (rarely transitional between “aa” and pahoehoe; such as the Berry Hill topset lavas) that alternate with thicker flows (up to 5 m in thickness) of massive lavas (*e.g.* at Southern Lachman

Crags). The subaerial lavas are slight to moderately vesiculated and in some places (e.g. at Lachman Crags) they contain multiple elliptical vesicle-rich pipes, vertical

veinlets and planar dyke-like injections defined by concentration of vesicles (Fig. 4d, e). Horizontally oriented columnar jointing is well developed at some outcrops.

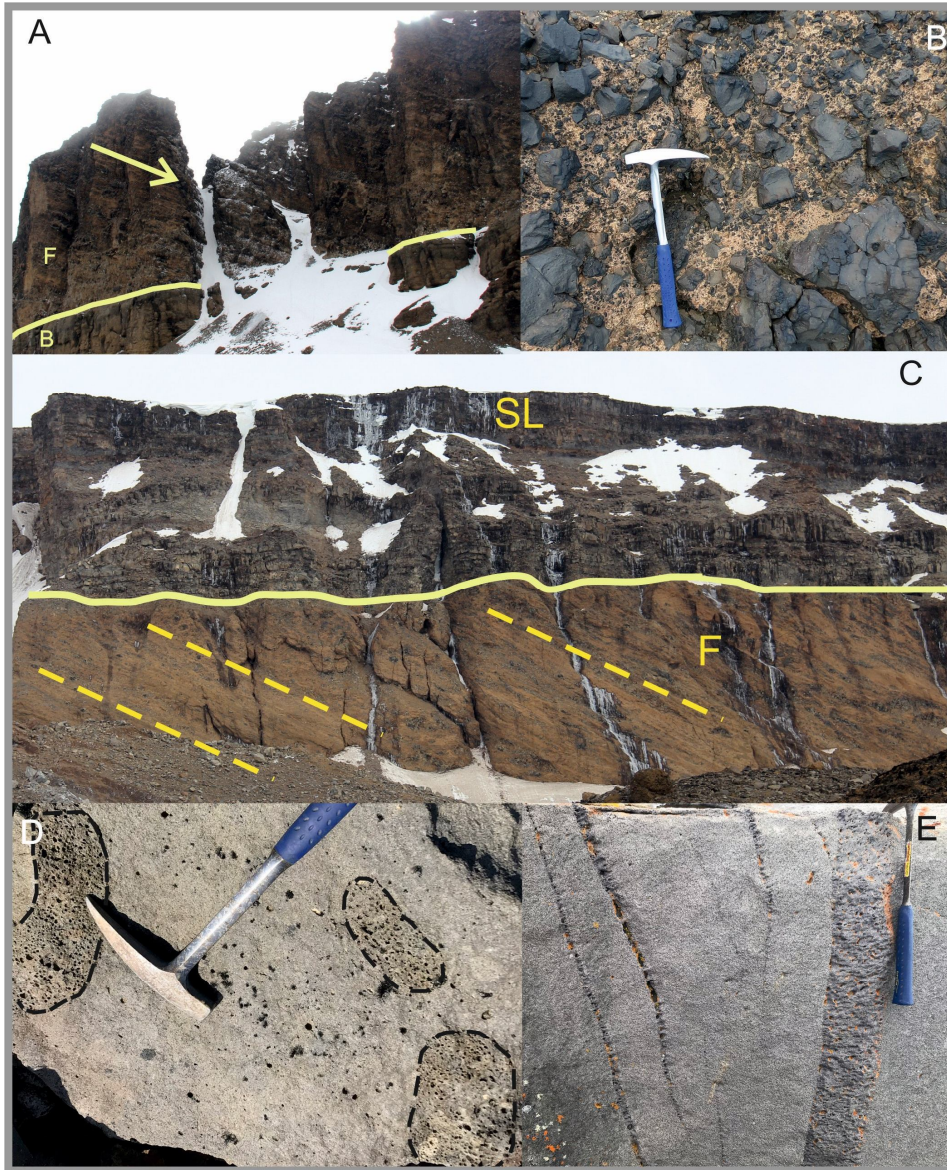


Fig. 4. A- Fine-medium grained sedimentary bottomset (B) overlain by foreset-bedded hyaloclastite breccias (F), eastern slopes of Berry Hill; B- Hyaloclastite breccia including dark angular pillow fragments. C- Steeply dipping foreset breccia (F) and overlying topset subaerial lavas (SL), southern Lachman Crags; D- Elliptical vesicle rich pipes and E- Vesicle- rich veinlets and dyke-like injections in subaerial lavas, southern Lachman Crags.

5. Petrography

The volcanic rocks investigated here belong to James Ross Island Volcanic Group. The volcanic occurrences from which the samples were collected include pillow lavas, pillow lava fragments within hyaloclastite breccias, feeder dykes and plugs

(chimneys), and sub-aerial lavas (with ultramafic xenoliths in some places) of the LCLFD and Cape Lachman lava-fed delta. Petrographic characteristics of individual rock types are summarised below.

5.1 Pillow lava

Pillow lavas can be easily distinguished from sub-aerial lavas with their distinct pilotaxitic and undercooling textures, as well as the lack of ultramafic xenoliths (Fig 5a). Olivine is the most abundant among the phenocryst in this rock type (95–98% of phenocrysts), and is accompanied by relatively less abundant clinopyroxene (3–5%) and plagioclase (labradorite-bytownite). Olivine phenocrysts mainly form euhedral and subhedral crystals with grain size up to 5 mm. In some cases, olivine phenocrysts exhibit disequilibrium features, such as embayed edges, skeletal textures, as well

as swallow-tails (Fig. 5a, b). In many cases, olivine phenocrysts contain minor Fe-Ti oxides. Clinopyroxene is an abundant phase in the groundmass, but is very scarce as phenocrysts. Their grain size is much smaller than olivines (<1 mm) and they are generally free of alteration. The lavas have fine-grained groundmass that consists of microlites and microcrystals of olivine and clinopyroxene with minor plagioclase and Fe-Ti oxides. Some pillow lavas display vesicular and amygdaloidal textures with the vesicles usually infilled by fibrous zeolite minerals.

5.2. Sub-aerial lava

The majority of the JRIVG basalts are represented by sub-aerial lavas. Compositionally, they are olivine basalts with distinct porphyritic and intersertal textures. They frequently contain mantle-derived ultramafic xenoliths as a distinctive feature. The basaltic samples display common petrographic characteristics: olivine is the main phenocryst and, similar to the pillow lavas, they contain minor clinopyroxene (3–4%) and plagioclase (labradorite-bytownite) in their phenocryst assemblages. The groundmass is generally fine grained and composed of plagioclase microlites and microcrysts of clinopyroxene and olivine. An important distinctive feature of the sub-aerial basalts is their disequilibrium textures such as sieve and embayed textures observed in olivine phenocrysts. Some of the olivine phenocrysts have rounded and corroded

edges and present clear embayment (Fig. 5c), which reflects a disequilibrium condition between the groundmass and phenocrysts. In some of the samples, olivine phenocrysts have a thin outer rim that is distinguished by its slightly different interference colour. This may be the result of a core to rim compositional variation of the crystal. In addition, amygdaloidal textures are exhibited in few samples from the sub-aerial lavas (Fig. 5c).

Ultramafic xenoliths carried to the surface by the magmas that form the sub-aerial lavas are mainly dunites and wehrlites in composition. They consist of 85–95% olivine, 5–15% clinopyroxene and 3–5% Fe-Ti oxides and display coarse-grained granular textures (Fig. 5d). Most of the olivines display deformation lamellae and undulose extinction.

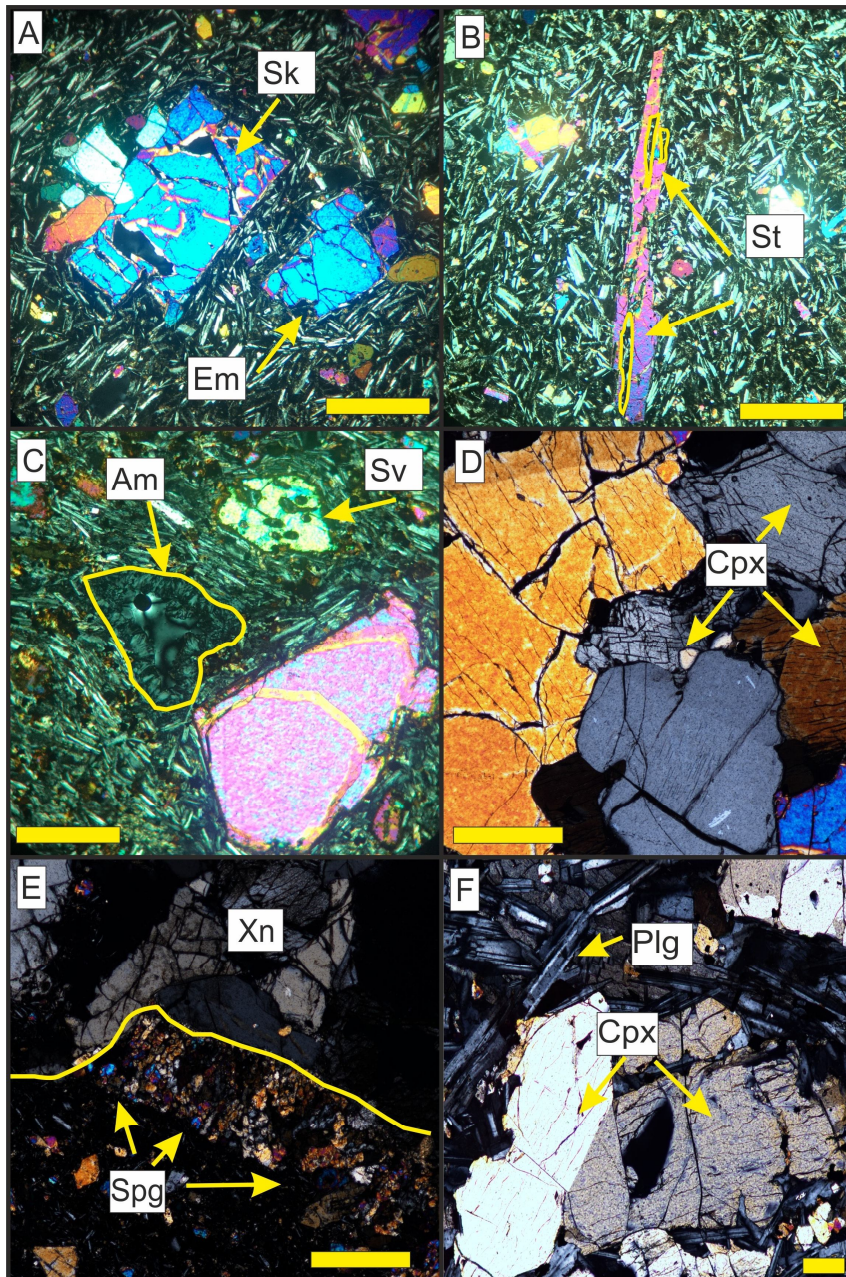


Fig. 5. Photomicrographs of JRIVG lavas and xenoliths (Scale 1mm); A- pilotaxitic texture of pillow lavas with skeletal olivine crystal and embayed texture; B- olivine crystal with swallow tails in pillow lava; C- intersertal texture of subaerial lavas with sieve textured olivine crystal and amygdoloidal texture; D- coarse-grained granular texture of xenoliths; E- spongy texture at the contact between xenolith and host rock F-Subophitic texture of dyke samples (Sk: skeletal, Em: embayed, St: swallow-tail, Am: amygdoloidal, Sv: sieve, Cpx: clinopyroxene, Xn: xenolith, Spg: spongy, Plg: plagioclase). All images in cross-polarized light (XPL).

At the very edge of the xenoliths, spongy texture defined by olivine and pyroxenes are common (Fig. 5e). In addition, serrated and indented rims of olivines and lack of triple junctions of the crystals with $\sim 120^\circ$ angles are significant indicators of reaction with the host basaltic melt. Moreover, the

boundaries between the xenoliths and the host basalts are characterized by serrated and indented edges instead of a sharp contact (Fig. 5e). Along with this zone, a very thin layer of tiny olivine grains has grown at the xenolith wall in addition to the spongy textures (Fig. 5e).

5.3. Dykes, sills, and plugs

This rock group has similar mineral compositions and inter-mineral textures to those observed in the pillow lavas and sub-aerial lava flow, but they are relatively coarser-grained and display sub-ophitic like textures defined by enclosing of pyroxene crystals by plagioclase laths (Fig. 5f).

The phenocryst composition of the dykes is olivine (85–95%), with minor clinopyroxene (5–10%) and plagioclase (7–10%). Plagioclase mainly forms as microcrystals and microliths, whereas olivine and clinopyroxene are represented by phenocrysts set in a microcrystalline groundmass.

6. Geochemical characteristics

The eruptive products we investigated are compositionally similar to those reported by Košler et al. (2009). Here, we provide additional data from different localities to improve our understanding of the geochemical characteristics of the whole volcanic suite of JRIVG. Geochemically no significant difference has been observed between the pillow lavas, the feeder dykes and plugs (chimneys) and the subaerial lavas. We, therefore, interpret the geochemical variations of all rock types together. The volcanic rocks from the JRIVG are mainly silica-poor mafic rocks with high MgO (5.02–11.34 wt. %) and total alkali ($K_2O + Na_2O = 4.32\text{--}6.59$ wt. %) contents (Table 1). The rocks are generally sodic alkaline in character as their Na_2O/K_2O ratios are in the range 2.28–4.17. They have moderate CaO (4.06–11.87 wt. %) and relatively high Al_2O_3 (14.80–16.60 wt. %) contents and their Cr and Ni concentrations vary from 113 to 379 ppm and from 32 to 244 ppm, respectively. With their low silica and high alkali contents the volcanic rock samples all plot in the alkaline

field of Irvine and Baragar (1971) and also classify as alkaline basalt and trachy-basalt in the TAS classification diagram of Le Bas et al. (1986) (Fig. 6).

The samples display a well-defined positive correlation between Ni (and Cr) and MgO indicating that olivine (possibly together with pyroxene) fractionation was particularly effective during differentiation of the magmas, while the negative covariance of Al_2O_3 with MgO suggest no significant effects of plagioclase fractionation. Although major and trace element variations for most of the volcanic rocks reflect variable effects of fractional crystallization, there are also some samples with relatively high MgO, Ni, and Cr contents, as well as high Mg# within a range that is in exchange equilibrium with mantle olivine, suggesting that they are closer to primary melt composition.

With their similar REE concentrations, the volcanic rock samples exhibit straight and more or less sub-parallel profiles on a chondrite-normalized (Boynnton 1984) REE diagram (Fig. 7a).

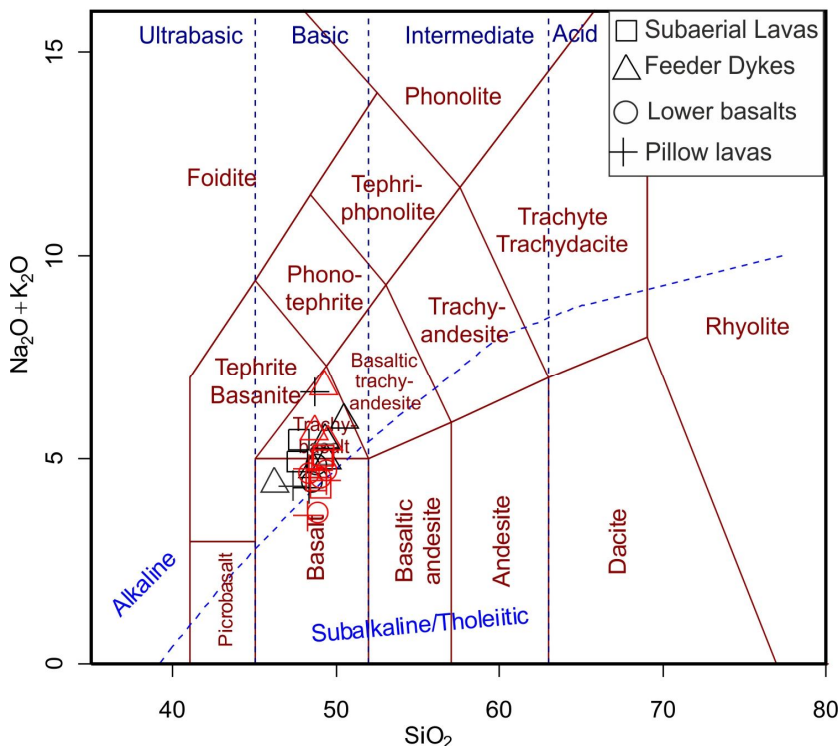


Fig. 6. Classification of the JRIVG lavas in the TAS diagram of LeBas *et al.* (1986). Data from Koşler *et al.* (2009) are plotted for comparison (shown as red symbols).

There is generally a well-defined correlation between REE abundances, and the samples display strong, but variable enrichments in LREE. La_N/Yb_N ratios of the samples range between 4.2 and 9.2 (the subscript N denotes chondrite normalized).

On a primitive mantle normalized (Sun *et McDonough* 1989) diagram, the volcanic rocks, in general, have all the classic enrichments in large-ion lithophile elements (LILE), high-field strength elements (HFSE) and light to medium rare earth elements (L-MREE) and slight relative depletion in heavy rare-earth elements (HREE) that characterize basalts from oceanic intra-plate suites, as well as continental rift settings (Fig. 7b). With these characteristics, the samples mostly exhibit typical ocean island basalt (OIB)-type element distributions. No samples show negative Ta or Nb

anomalies, indicating derivation from a mantle source(s) with no subduction component and an ascent of primary melt(s) with no significant crustal contamination. The geochemical characteristics of these basalts of intra-plate origin are, to a first order, consistent with melt generation by melting of geochemically enriched (in terms of incompatible elements) component, most probably in association with continental extensional processes.

Consistent with the interpretations from the normalized element plots, the rocks mostly classify as within plate basalt in a ternary element plot of Hf–Th–Ta (Wood 1980), as the samples mostly plot close to the dividing line between the within-plate alkaline and the within-plate tholeiite fields (Fig. 8).

LITHOSTRATIGRAPHY AND PETROLOGY OF LAVA-FED DELTAS IN JAMES ROSS ISLAND

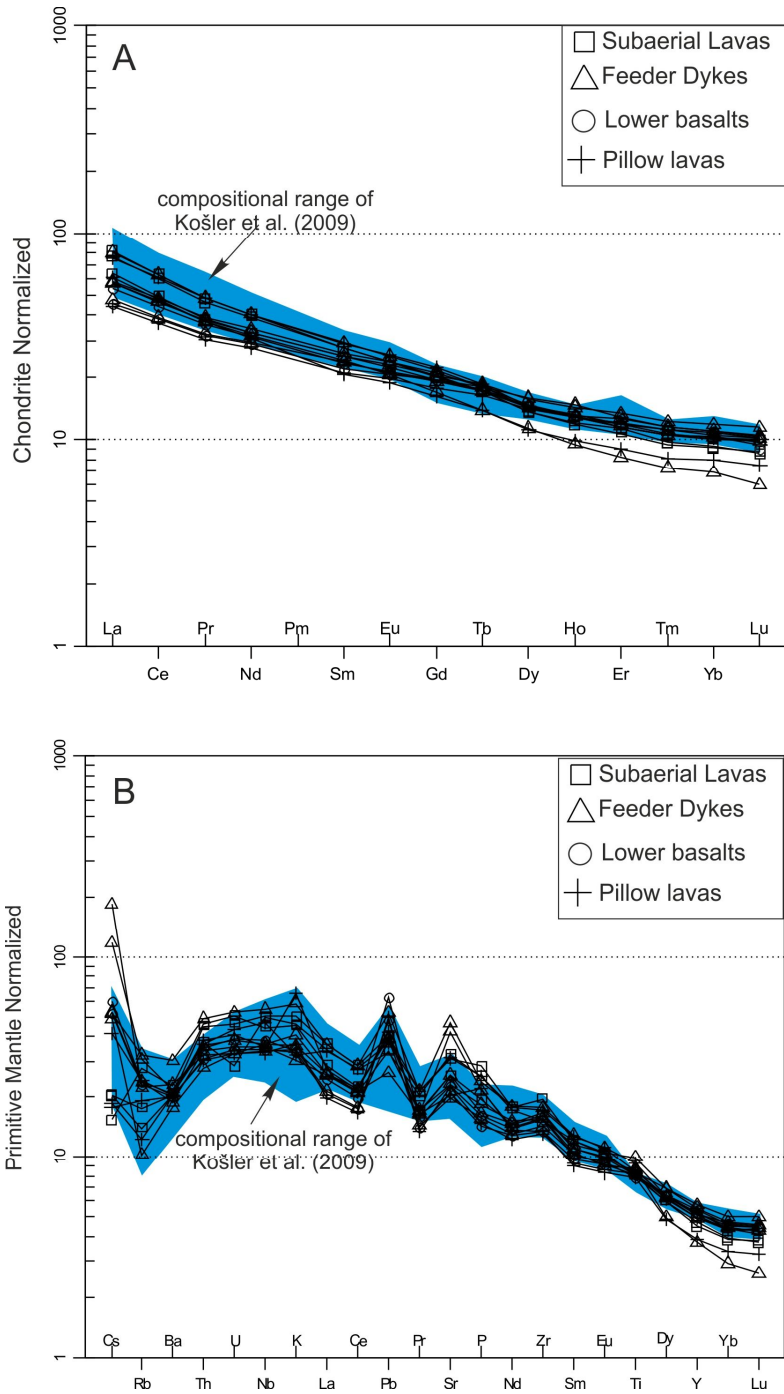


Fig. 7. (A) Chondrite- and (B) Primitive Mantle (PM)-normalized trace element patterns for the JRIVG lavas. Chondrite and PM normalizing values are from Boynton (1984) and Sun et McDonough (1989), respectively.

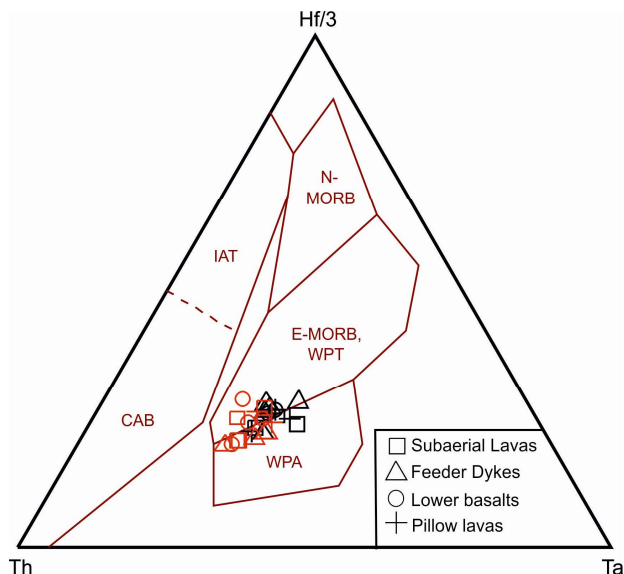


Fig. 8. Hf – Th – Ta diagram (Wood 1980) showing the basaltic rocks of the JRIVG with respect to the fields for within-plate alkaline (WPA), within-plate tholeiite (WPT), calc-alkaline basalt (CAB), island arc tholeiite (IAT), and normal (N)-MORB and enriched (E)-MORB. Symbols correspond to Fig. 6.

7. Petrogenetic considerations

Relative abundances of incompatible trace elements with similar incompatibilities provide important information about mantle source variations and permit determination of the relative importance of different processes (*e.g.* partial melting, source metasomatism and contamination of melts by crustal material) in shaping the compositions and geochemical characteristics of mantle-derived melts. An assessment of incompatible trace element behaviour of the volcanic rocks has been performed here to define the nature and composition of the source of the lavas using the Th and Ta concentrations with Yb used as a normalizing factor to minimize the effects of fractional crystallization and crystal accumulation (*e.g.* Pearce *et al.* 2005).

Intra-plate type geochemical signatures of the lavas are highlighted in Fig. 9, where the Th/Yb vs. Ta/Yb variations define a compositional space within the typi-

cal MORB–OIB mantle array for all the volcanic rocks investigated in this study, indicating that the mantle source, from which the magmas were originated had no subduction component and the resulting magmas were not affected by any significant contamination of crustal material. This may indicate a rapid ascent of the mantle-derived melts to the surface without significant compositional modifications in shallow magma chambers. Rapid movement of the melts in the melt channels is also evident from the existence of abundant mantle-derived ultramafic xenoliths found particularly in some subaerial basaltic lavas. However, high values of both Ta/Yb and Th/Yb ratios, which are commonly observed in OIB-type intra-plate lavas, may be explained by a number of processes including magma generation by: (1) small degrees of melting of a convectively homogenized source that is enriched in-

compatible elements relative to depleted MORB source; or (2) small degrees of partial melting of a mantle source that leaves garnet-bearing residue; or (3) sys-

tematic mixing between increments of melt derived from a compositionally uniform source by variable degrees of melting.

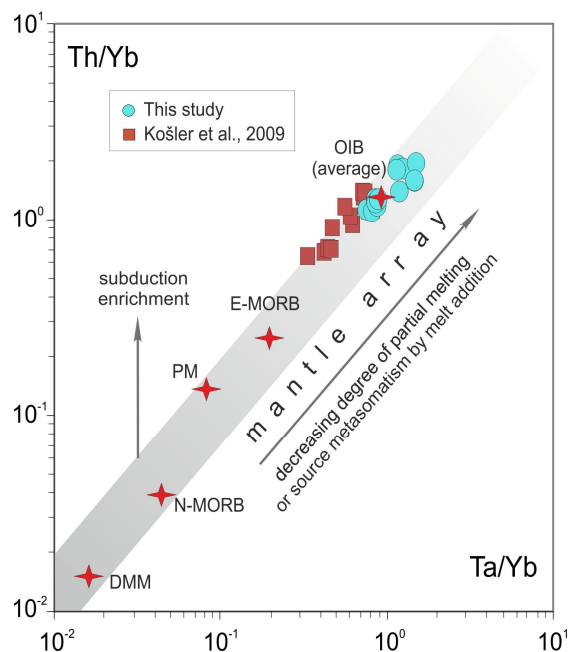


Fig. 9. Th/Yb vs. Ta/Yb log-log diagram for the JRIVG rocks. Also plotted for comparison are some typical oceanic basaltic and mantle compositions including the depleted MORB mantle (DMM), primitive mantle (PM), N-MORB and E-MORB. End-member compositions are from Sun et McDonough (1989).

In an attempt to characterize the nature of the mantle source in terms of geochemical and mineralogical compositions, we applied semi-quantitative modelling using the approach described in Aldanmaz et al. (2006). On a plot of La/Sm vs. La, where we compare the compositions of the volcanic rocks from JRIVG with those obtained from theoretically calculated melt compositions, the samples all define a compositional trend characterized by higher LREE/MREE ratios compared to magma compositions formed by melting of a typical asthenospheric upper mantle material (Fig. 10). The results show that the magmas forming the alkaline volcanic rocks of JRIVG are unlikely to have been derived

from a source similar in composition to the typical asthenospheric upper mantle that is characterized by significant depletion in more incompatible to less incompatible element ratios (shown as DMM). Unlike this ambient asthenospheric source, the mantle region, from which the within-plate type basaltic rocks of JRIVG originated, appears to have been enriched in La, concentrations and La/Sm ratios. In order to extend the modelling further to estimate the degree of partial melting and the trace element composition of the source mantle independently, we have applied the dynamic melting inversion method using the parameters described in Aldanmaz et al. (2006).

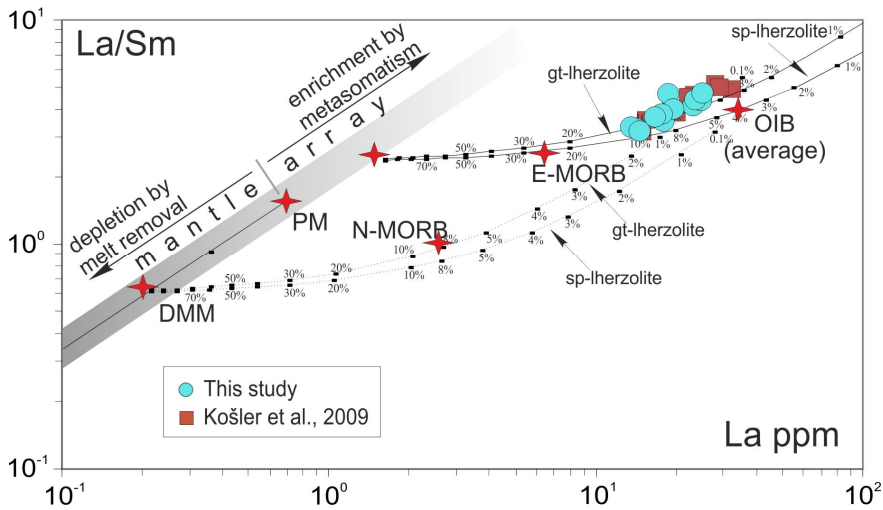


Fig. 10. Plot of La/Sm vs. La for the comparison of the JRIVG lava compositions with the melt curves (or lines) obtained using the non-modal batch melting equations. Melt curves are drawn using the parameters described in Aldanmaz *et al.* (2006). End-member compositions are as in Fig. 9.

Element	Di	Pi	Alkali Bas. JR102	Alkali Bas. JR104	Qi	DMI		Co (ppm)	(Co) _N
						f1 (%)	f2 (%)		
La	0.0057	0.0373	13.62	23.73	0.57	2.37	6.06	1.02	4.34
Ce	0.0103	0.0676	29.65	48.37	0.61	3.11	7.73	2.20	3.64
Pr	0.0178	0.1039	3.73	5.60	0.67	2.60	6.59	0.28	3.18
Nd	0.0259	0.1457	16.55	23.37	0.71	3.70	9.07	1.26	2.79
Sm	0.0422	0.1828	4.10	5.39	0.76	2.68	6.94	0.34	2.28
Average						2.89	7.28		

Table 2. Estimation of partial melting degrees and mantle source composition for alkali basalts from the JRIVG. *Symbols:* DMI = CR (Concentration Ratio) method for dynamic melting, f = degree of partial melting, Di = bulk distribution coefficients; Qi = enrichment concentration ratio; Co = source concentration; (Co)_N = chondrite normalized Co concentrations.

The results are presented in Table 2, where it can be seen that there is generally a good agreement between the estimated degrees of partial melting for most of the incompatible elements, although the exceptions are the HREE, which behave compatibly in the presence of garnet as one of the residual phases during melting. The average estimates based on the calculations using the LREE concentrations of the most primary lava compositions have been obtained as 2.9–7.3% for the alkaline basaltic

rocks from the JRIVG, indicating that the melts forming the lavas in this region are the products of relatively small degrees of partial melting.

The source concentrations for the mafic alkaline volcanic rocks were also estimated using these two different degrees of partial melting, assuming that the lavas forming this suite are co-genetic. The results are plotted on a chondrite-normalized REE diagram (Fig. 11).

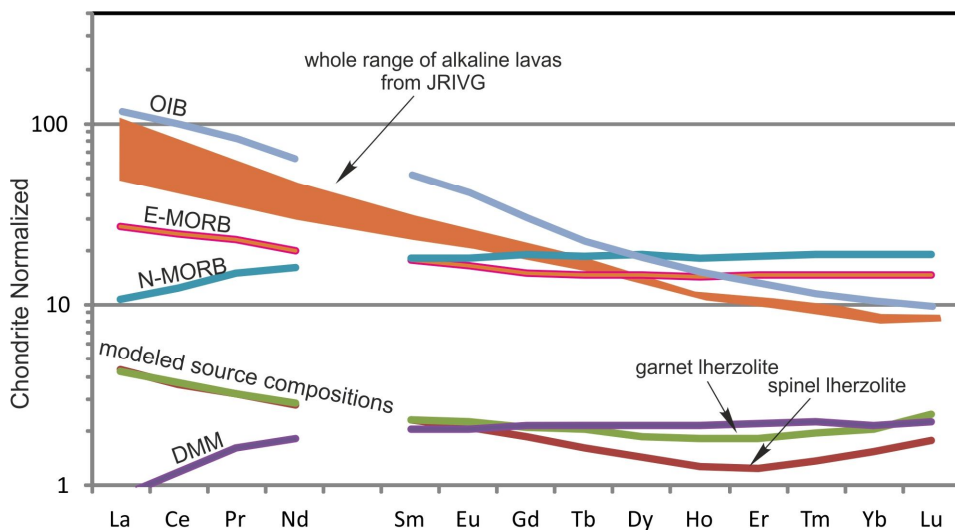


Fig. 11. Chondrite-normalized REE patterns showing the likely mantle source compositions calculated by dynamic melting inversion (DMI) method (Zou, 1998) using the data from the JRIVG lavas. The modelling uses the enrichment ratios of two different incompatible elements between two different, but cogenetic primary magmas and the parameters described in Aldanmaz et al. (2006). End-member compositions are as in Fig. 9. Normalizing values are from Boynton (1984).

Also plotted for comparison are the compositions that represent the Depleted MORB Mantle (DMM), NMORB, EMORB and OIB. It should be noted that the concentrations of the LREE are not affected by whether the source is garnet or spinel lherzolite, whereas the M-HREE are affected significantly by the source mineralogy. The estimated source concentrations range from 2.3–3.6 times chondrite for the LREEs, to 1.7–2.4 times chondrite for the HREEs when the source composition is taken as garnet lherzolite, which is evident from the depleted HREE/LREE ratios of most of the lava compositions.

The results also indicate that the estimated LREE concentrations of the mantle source are always greater than those of the

Depleted MORB Mantle (DMM) composition as they range from 4.9 (La) to 1.5 (Nd) times the DMM. On the other hand, the M-HREE may be similar to those of the DMM depending on the modal mineralogy of the source. This indicates that the magmas forming the volcanic rocks are unlikely to have been derived from a source similar in composition to the average normal-type MORB source, which is characterized by significant depletion in more incompatible element ratios. However, unlike the MORB source, the source region from which the within-plate type basaltic rocks of JRIVG originated appears to have been significantly enriched in more incompatible elements.

8. Discussion

The preliminary investigations and the evaluation of the geochemical data suggest that the basaltic volcanic rocks from JRIVG exhibit geochemical signatures closely resembling those of Na-rich, continental intra-plate alkaline suites worldwide, the formation of which are in many cases attributed to incompatible trace element enriched source components generated by localized metasomatic processes (Aldanmaz *et al.* 2006, Jung *et al.* 2011). This type of lava compositions is particularly common in tectonic settings characterized by an earlier stage of plate convergence followed by a later stage of lithospheric extension (Li *et al.* 2016, Chen *et al.* 2017). Melt generation in these environments is generally considered to be the result of adiabatic decompression in association with lithospheric extension-driven passive upwelling of the upper mantle material. The enriched component that undergoes partial melting during extension to produce the intra-plate geochemical signatures, on the other hand, is widely interpreted to be related to metasomatic processes through material addition during preceding stage(s) of plate convergence and recycling (Kimura *et al.* 2016). For the case of the volcanic rocks of the JRIVG these two sequential geodynamic events may be represented by (1) the earlier subduction of the Phoenix plate beneath the Antarctic Peninsula along the South Shetland trench (Herron *et Tucholke* 1976, Barker 1982, Saunders *et al.* 1982) and (2) the lithospheric extension that has been operational since the Latest Miocene (Saunders *et Tarney* 1982, Smellie *et al.* 1984).

Recycled slab-derived components are known to affect mantle compositions in a number of discrete ways (Stixrude *et Lithgow-Bertelloni* 2012, Kimura *et al.* 2016). In this context, trace element compositional diversity observed in mantle sources of intra-plate basaltic suites is in some cases attributed to the variable involvement of subducted oceanic crustal material (Hof-

mann 1997, Day *et al.* 2009). Recent experimental studies have shown that many of the features regarding the geochemical compositions of intra-plate basalt suites cannot be explained by melt generation from homogeneous, volatile-free peridotite compositions (Dasgupta *et al.* 2006). In particular, the common appearance of residual garnet signature, as well as the evidence for the requirement of volatile-rich melts in the vast majority of intra-plate basalt suites have motivated many researchers to suggest that melts originated from carbonated eclogite or pyroxenite play an important role in generating the metasomatically altered zones within the peridotitic upper mantle, which eventually melted to produce magmas with typical intra-plate geochemical signatures (Schiano *et al.* 1994, Dasgupta *et al.* 2006).

Direct melting of subducted oceanic crust is unlikely to produce melts similar in compositions to those of intra-plate alkaline basalts because high degrees of partial melting of eclogite or pyroxenite source will produce melts with higher silica and lower magnesium content than observed in intra-plate basaltic magmas in general (Yaxley *et Green* 1998, Dasgupta *et al.* 2006). However, carbonated silicate melts generated by melting of oceanic crustal material are usually considered to have the ability to react with the surrounding peridotites within the mantle to form modally metasomatized domains displaying strong compositional heterogeneities with particular enrichments in highly incompatible trace elements (Yaxley *et Green* 1998, Kiseeva *et al.* 2013). Such compositionally distinct patches in the peridotite matrix have been shown to have the capacity to form nepheline-normative melts with relatively enriched incompatible trace element concentrations than the typical MORB lavas (Mallik *et Dasgupta* 2013). Therefore, the interaction between melts of a slab-derived component and ambient peri-

dotitic mantle appears to be a viable explanation for the geochemically distinct metasomatic domains within the upper mantle that are sampled by the intra-plate type alkaline melts forming the post-latest Miocene lavas of the JRIVG.

References

- ALDANMAZ, E., KÖPRÜBAŞI, N., GÜRER, Ö. F., KAYMAKÇI, N. and GOURGAUD, A. (2006): Geochemical constraints on the Cenozoic, OIB-type alkaline volcanic rocks of NW Turkey: implications for mantle sources and melting processes. *Lithos*, 86: 50-76.
- BARKER, P. F. (1982): The Cenozoic subduction history of the Pacific margin of the Antarctic Peninsula: Ridge crest-trench interactions. *Journal of the Geological Society, London*, 139: 787-801.
- BARKER, D. H. N., CHRISTENSON, G. L., AUSTIN, J. A. and DALZIEL, I. W. D. (2003): Backarc basin evolution and cordilleran orogenesis: Insights from new ocean-bottom seismograph refraction profiling in Bransfield Strait, Antarctica. *Geology*, 31: 107-110.
- BASTÍAS, J., HERVÉ, F., FUENTES, F., SCHILLING, M., POIRON, A. and GUTIÉRREZ, F. (2012): Mantle xenoliths found at Santa Martha cove, James Ross Island, Antarctica. *13° Congreso Geológico Chileno, Actas: 365-367*, Antofagasta.
- BIBBY, J. S. (1966): The stratigraphy of part of north-east Graham Land and the James Ross Island group. *British Antarctic Survey Scientific Reports*, No. 53: pp. 1-37.
- BOYNTON, W.V. (1984): Geochemistry of the rare earth elements: meteorite studies. In: P. Henderson (ed.): *Rare Earth Element Geochemistry*. Elsevier, pp. 63-114.
- CALABOZO, F. M., STRELIN, J. A., ORIHASHI, Y., SUMINO, H. and KELLER, R. A. (2015): Volcano-ice-sea interaction in the Cerro Santa Marta area, northwest James Ross Island, Antarctic Peninsula. *Journal of Volcanology and Geothermal Research*, 297: 89-108.
- CHEN, H., XIA, Q. K., INGRIN, J., DELOULE, E. and BI, Y. (2017): Heterogeneous source components of intraplate basalts from NE China induced by the ongoing Pacific slab subduction. *Earth and Planetary Science Letters*, 459: 208-220.
- CRAME, J. A., PIRRIE, D., RIDING, J. B. and THOMSON, M. R. A. (1991): Campanian-Maastrichtian (Cretaceous) stratigraphy of the James Ross Island area, Antarctica. *Journal of the Geological Society, London*, 148: 1125-1140.
- DASGUPTA, R., HIRSCHMANN, M. M. and STALKER, K. (2006): Immiscible transition from carbonate-rich to silicate-rich melts in the 3 GPa melting interval of eclogites + CO₂ and genesis of silica-undersaturated ocean island lavas. *Journal of Petrology*, 47: 647-671.
- DAY, J. M. D., PEARSON, D. G., MACPHERSON, C. G., LOWRY, D. and CARRACEDO, J.-C. (2009): Pyroxenite-rich mantle formed by recycled oceanic lithosphere: oxygen-osmium isotope evidence from Canary Island lavas. *Geology*, 37: 555-558.
- DEL VALLE, R. A. and SCASSO, R. A. (2004): Límite de la cuenca Larsen en la península Tabarin, Antártida. *Revista de la Asociación Geológica Argentina*, 59(1): 38-44.
- EDWARDS, B. R., RUSSELL, J. K. and ANDERSON, R. G. (2002): Subglacial, phonolitic volcanism at Hoodoo Mountain volcano, northwestern Canadian Cordillera. *Bulletin of Volcanology*, 64: 254-272.
- HAMBREY, M. J., SMELLIE, J. L., NELSON, A. E. and JOHNSON, J. S. (2008): Late Cenozoic glacier volcano interaction on James Ross Island and adjacent areas, Antarctic Peninsula region. *Geological Society of America Bulletin*, 120 (5/6): 709-731.
- HERRON, E. M., TUCHOLKE, B. E. (1976): Sea-floor magnetic patterns and basement structure in the southeastern Pacific. In: C.D. Hollister et al. (eds.): *Initial Reports of the Deep Sea Drilling Project*, 35, U.S. Government Printing Office, Washington D.C., pp. 263-278.
- HOFMAN, A. W. (1997): Mantle geochemistry: the message from oceanic volcanism. *Nature*, 385:219-229.
- IRVINE, T. N., BARAGAR, W. R. A. (1971): A guide to the chemical classification of the common volcanic rocks. *Canadian Journal of Earth Sciences*, 8: 448-523.

- JANOÚŠEK, V., FARROW, C. M. and ERBAN, V. (2006): Interpretation of whole-rock geochemical data in igneous geochemistry: introducing Geochemical Data Toolkit (GCDkit). *Journal of Petrology*, 47 (6): 1255-1259.
- JONES, J. G., NELSON, P. H. H. (1970): Flow of basalt lava from air into water. Its structural expression and stratigraphic significance. *Geological Magazine*, 107: 13-19.
- JONKERS, H.A., LIRIO, J.M., DEL VALLE, R.A. and KELLEY, S.P. (2002): Age and environment of Miocene–Pliocene glaciomarine deposits, James Ross Island, Antarctica. *Geological Magazine*, 139: 577-594.
- JUNG, S. PFÄNDER, J.A. BRAUNS, M. and MAAS, R. (2011): Crustal contamination and mantle source characteristics in continental intra-plate volcanic rocks: Pb, Hf and Os isotopes from central European volcanic province basalts. *Geochimica et Cosmochimica Acta*, 75: 2664-2683.
- KIMURA, J.-I., GILL, J. B., SKORA, S., VAN KEKEN, P. E. and KAWABATA H. (2016): Origin of geochemical mantle components: Role of subduction filter. *Geochemistry, Geophysics, Geosystems*, 17: 3289-3325, doi:10.1002/2016GC006343.
- KISEEVA, E. S., LITASOV, K. D., YAXLEY, G. M., OHTANI, E. and KAMENETSKY, V. S. (2013): Melting and phase relations of carbonated eclogite at 9–21 GPa and the petrogenesis of alkali rich melts in the deep mantle. *Journal of Petrology*, 54 (8): 1555-1583.
- KOŠLER, J., MAGNA, T., MLČOCH, B., MIXA, P., NÝVLT, D. and HOLUB, F. V. (2009): Combined Sr, Nd, Pb and Li isotope geochemistry of alkaline lavas from northern James Ross Island (Antarctic Peninsula) and implications for back-arc magma formation. *Chemical Geology*, 258: 207-218.
- KRISTJÁNSSON, L., GUDMUDSSON M. T., SMELLIE, J. L., MCINTOSH, W. C. and ESSER, R. (2005): Palaeomagnetic, ³⁹Ar/⁴⁰Ar, and stratigraphical correlation of Miocene–Pliocene basalts in the Brandy Bay area, James Ross Island, Antarctica. *Antarctic Science*, 17 (3): 409-417.
- LARTER, R. D., BARKER, P.F. (1991): Effects of the ridge crest-trench interaction on Antarctic-Phoenix spreading: forces on a young subduction plate. *Journal of Geophysical Research*, 96: 19 583-19 607.
- LAWVER, L. A., KELLER, R. A., FISK, M. R. and STRELIN, J. (1995): Bransfield Strait, Antarctic Peninsula: active extension behind a dead arc. In: B. Taylor. (ed.): Backarc Basins: Tectonics and Magmatism. Plenum Press, Holland, 315-342.
- LE BAS, M.J., LE MAITRE, R.W., STRECKEISEN, A. and ZANETTIN, B., (1986): A chemical classification of volcanic rocks based on the total alkali-silica diagram. *Journal of Petrology*, 27: 445-450.
- LE MASURIER, W.E., (2002): Architecture and evolution of hydrovolcanic deltas in Marie Byrd Land, Antarctica. In: J.L. Smellie, M.G. Chapman (eds.): Volcano-ice Interaction on Earth and Mars, *Geological Society of London Special Publications*, London, pp. 115-148.
- LI, H. Y., XU, Y. G., RYAN, J. G., HUANG, X. L., REN, Z. Y., GUO, H. and NING, Z.G. (2016): Olivine and melt inclusion chemical constraints on the source of intracratonic basalts from the eastern North China Craton: Discrimination of contributions from the subducted Pacific slab. *Geochimica et Cosmochimica Acta*, 178: 1-19.
- MALLIK, A., DASGUPTA, R. (2013): Reaction between MORB-eclogite derived melts and fertile peridotite and generation of ocean island basalts. *Earth and Planetary Science Letters*, 329–330: 97-108.
- MARENSSI, S. A., CASADÍO, S. and SANTILLANA, S. N. (2010): Record of Late Miocene glacial deposits on Isla Marambio (Seymour Island), Antarctic Peninsula. *Antarctic Science*, 22: 193-198.
- MASSABIE, A. C., MORELLI, J. R. (1977): Buchitas de la isla Vicecomodoro Marambio, Sector Antártico Argentino. *Revista de la Asociación Geológica Argentina*, 32: 44-51.
- MITCHELL, N. C., BEIER, C., ROSIN, P. L., QUARTAU, R. and TEMPERA, F. (2008): Lava penetrating water: Submarine lava flows around the coasts of Pico Island, Azores. *Geochemistry, Geophysics, Geosystems*, 9: 29, <http://dx.doi.org/10.1029/2007gc001725>.
- MLČOCH, B., NÝVLT, D. (2013): Vulkanismus a zalednění prostoru ostrova Jamese Rosse. In: P. Prošek (ed.): ANTARKTIDA. Academia Press, pp. 253-264.

LITHOSTRATIGRAPHY AND PETROLOGY OF LAVA-FED DELTAS IN JAMES ROSS ISLAND

- MLČOCH, B., NÝVLT, D. and MIXA, P. eds. (2018): Geological map of James Ross Island - northern part 1:25,000. Unpublished manuscript, Czech Geological Survey, Praha.
- NELSON, P. H. H. (1975): The James Ross Island Volcanic Group of North–East Graham Land. *British Antarctic Survey Scientific Report*, 54: 62 pp.
- NELSON, A.E., SMELLIE, J.L., HAMBREY, M.J., WILLIAMS, M., VAUTRAVERS, M., SALZMANN, U., MCARTHUR, J. M. and REGELOUS, M. (2009): Neogene glacial debris flows on James Ross Island, northern Antarctic Peninsula, and their implications for regional climate history. *Quaternary Science Reviews*, 28: 3138-3160.
- NEHYBA, S., NÝVLT, D. (2014): Deposits of pyroclastic mass flows at Bibby Hill (Pliocene, James Ross Island, Antarctica). *Czech Polar Reports*, 4: 103-122.
- NEHYBA, S., NÝVLT, D. (2015): “Bottomsets” of the lava–fed delta of James Ross Island Volcanic Group, Ulu Peninsula, James Ross Island, Antarctica. *Polish Polar Research*, 36: 1-24.
- NÝVLT, D., KOŠLER, J., MLČOCH, B., MIXA, P., LISÁ, L., BUBÍK, M. and HENDRIKS, B. W. H. (2011): The Mendel Formation: evidence for Late Miocene climatic cyclicity at the northern tip of the Antarctic Peninsula. *Palaeogeography, Palaeoclimatology, Palaeoecology*, 299: 363-384.
- PEARCE, J. A., STERN, R. J., BLOMMER, S. H. and FRYER, P. (2005): Geochemical mapping of the Mariana arc basin system: implication for the nature and distribution of the subduction component. *Geochemistry Geophysics Geosystems* 6, article no: Q07006, 27 pp., doi: 10.1029/2004GC000895.
- PIRRIE, D., SYKES, M. A. (1987): Regional significance of proglacial delta front reworked tuffs, James Ross Island area. *British Antarctic Survey Bulletin*, 77: 1-12.
- POREBSKI, S. J., GRADZINSKI, R. (1990): Lava–fed Gilbert delta in the Polonez Cove Formation (Lower Oligocene), King George Island, West Antarctica. In: A. Colella, D.B. Prior (eds.): Coarse–Grained Deltas. *International Association of Sedimentologists Special Publication*, 10: 335-351.
- REX, D. C. (1976): Geochronology in relation to the stratigraphy of the Antarctic Peninsula. *British Antarctic Survey Bulletin*, 43: 49-58.
- SAUNDERS, A. D. (1982): Petrology and geochemistry of alkali basalts from Jason Peninsula, Oscar II Coast, Graham Land. *British Antarctic Survey Bulletin*, 55: 1-19.
- SAUNDERS, A. D., TARNEY, J. (1982): Igneous activity in the southern Andes and northern Antarctic Peninsula: a review. *Journal of Geological Society, London*, 139: 691-700.
- SCHIANO, P., CLOCCHIATTI, R., SHIMIZU, N., WEIS, D. and MATTIELLI, N. (1994): Cogenetic silica-rich and carbonate-rich melts trapped in mantle minerals in Kerguelen ultramafic xenoliths: implications for metasomatism in the oceanic upper mantle. *Earth and Planetary Science Letters*, 123: 167-178.
- SIGVALDASON, G. (1968): Structure and products of subaquatic volcanoes in Iceland. *Contributions to Mineralogy and Petrology*, 18: 1-16.
- SKILLING, I. P. (1994): Evolution of an englacial volcano: Brown Bluff Antarctica. *Bulletin of Volcanology*, 56: 573-591.
- SKILLING, I. P. (2002): Basaltic pahoehoe lava–fed deltas: large–scale characteristics, clast generation, emplacement processes and environmental discrimination. In: J. L. Smellie, M. G. Chapman (eds.): Volcano–Ice Interaction on Earth and Mars. *Geological Society, London Special Publication*, 202: 91-113.
- SKILLING, I. P. (2009): Subglacial to emergent basaltic volcanism at Hlöðufell, south-west Iceland: a history of ice confinement. *Journal of Volcanology and Geothermal Research*, 185: 276-289.
- SMELLIE, J. L. (1987): Geochemistry and tectonic setting of alkaline volcanic rocks in the Antarctic Peninsula: a review. *Journal of Volcanology and Geothermal Research*, 32: 269-285.
- SMELLIE, J. L. (1999): Lithostratigraphy of Miocene–Recent, alkaline volcanic fields in the Antarctic Peninsula and eastern Ellsworth Land. *Antarctic Science*, 11: 362-378.
- SMELLIE, J. L. (2006): The relative importance of supraglacial versus subglacial meltwater escape in basaltic subglacial tuya eruptions: an unresolved conundrum. *Earth-Science Reviews*, 74: 241-268.
- SMELLIE, J. L., EDWARDS, B. R. (2016): Glaciovolcanism on Earth and Mars. Products, Processes and Palaeoenvironmental Significance. Cambridge University Press, 490 p.

- SMELLIE, J. L., SKILLING, I. P. (1994): Products of subglacial volcanic eruptions under different ice thicknesses: two examples from Antarctica. *Sedimentary Geology*, 91: 115-129.
- SMELLIE, J. L., PANKHURST, R., THOMSON, M. R. A. and DAVIES, R. E. S. (1984): The geology of the South Shetland Islands: VI. Stratigraphy, geochemistry and evolution (Vol. 87). British Antarctic Survey, 85 pp.
- SMELLIE, J. L., JOHNSON, J. S. and NELSON A.E. (2013): Geological map of James Ross Island. I. James Ross Island Volcanic Group (1:125 000 Scale). BAS GEOMAP 2 Series, Sheet 5, British Antarctic Survey, Cambridge.
- SMELLIE, J. L., MCARTHUR, J. M., MCINTOSH, W. C. and ESSER R. (2006): Late Neogene interglacial events in the James Ross Island region, Northern Antarctic Peninsula, dated by Ar/Ar and Sr-isotope stratigraphy. *Palaeogeography, Palaeoclimatology, Palaeoecology*, 242: 169-187.
- SMELLIE, J. L., JOHNSON, J. S., MCINTOSH, W. C., ESSER, R., GUDMUNDSSON, M. T., HAMBREY, M. J. and VAN WYK DE VRIES, B. (2008): Six million years of glacial history recorded in volcanic lithofacies of the James Ross Island Volcanic Group, Antarctic Peninsula. *Palaeogeography, Palaeoclimatology, Palaeoecology*, 260: 122-148.
- STIXRUDE, L., LITHGOW-BERTELLONI, C. (2012): Geophysics of chemical heterogeneity in the mantle. *Annual Review of Earth and Planetary Sciences*, 40: 569-595.
- SUN, S.-S., MCDONOUGH, W. F. (1989): Chemical and isotopic systematics of oceanic basalts: implications for mantle composition and processes. In: A. D. Saunders & M. J. Norry (eds.): *Magmatism in the Ocean Basins, Geological Society, London, Special Publication no. 42*, pp. 313-45.
- SYKES, M.A. (1988): New K–Ar age determinations on the James Ross Island Volcanic Group, north-east Graham Land, Antarctica. *British Antarctic Survey Bulletin*, 80: 51-56.
- TUFFEN, H., MCGARVIE, D. W., GILBERT, J. S. and PINKERTON, H. (2002): Physical volcanology of a subglacial-to-emergent rhyolitic tuya at Rauðu-fossafjöll, Torfajökull, Iceland. In: J. L. Smellie, M. G. Chapman (eds.): *Volcano-Ice interaction on Earth and Mars. Geological Society, London, Special Publications*, 202: 213-236
- UMINO, S., NONAKA, M. and KAUAHIKAUA, J. (2006): Emplacement of subaerial pahoehoe lava sheet flows into water: 1990 Kūpaianaha flow of Kilauea volcano at Kaimū Bay, Hawaii. *Bulletin of Volcanology*, 69: 125-139.
- WOOD, D. A. (1980): The application of a Th–Hf–Ta diagram to problems of tectonomagmatic classification and to establishing the nature of crustal contamination of basaltic lavas of the British tertiary volcanic province. *Earth and Planetary Science Letters*, 50: 11-30.
- WILCH, T. I., MCINTOSH, W. C. (2007): Miocene-Pliocene ice-volcano interactions at monogenetic volcanoes near Hobbs Coast, Marie Byrd Land, Antarctica. *US Geological Survey*, OF-2007-1047 doi:10.3133/of2007-1047.sep074
- YAXLEY, G., GREEN, D. (1998): Reactions between eclogite and peridotite: mantle refertilisation by subduction of oceanic crust. *Schweizerische Mineralogische und Petrographische Mitteilungen* 78: 243-255.